

## ARTICLE OPEN



# Forecasting the El Niño type well before the spring predictability barrier

Josef Ludescher<sup>1</sup>✉, Armin Bunde<sup>2</sup> and Hans Joachim Schellnhuber<sup>1</sup>

El Niño events represent anomalous episodic warmings, which can peak in the equatorial Central Pacific (CP events) or Eastern Pacific (EP events). The type of an El Niño (CP or EP) has a major influence on its impact and can even lead to either dry or wet conditions in the same areas on the globe. Here we show that the difference of the sea surface temperature anomalies between the equatorial western and central Pacific in December enables an early forecast of the type of an upcoming El Niño ( $p$ -value  $< 10^{-3}$ ). Combined with a previously introduced climate network-based approach that allows to forecast the onset of an El Niño event, both the onset and type of an upcoming El Niño can be efficiently forecasted. The lead time is about 1 year and should allow early mitigation measures. In December 2022, the combined approach forecasted the onset of an EP event in 2023.

*npj Climate and Atmospheric Science* (2023)6:196; <https://doi.org/10.1038/s41612-023-00519-8>

## INTRODUCTION

El Niño events are part of the El Niño-Southern Oscillation (ENSO)<sup>1–6</sup>, which can be perceived as a self-organized quasi-periodic pattern in the tropical Pacific ocean-atmosphere system, featured by rather irregular warm (“El Niño”) and cold (“La Niña”) excursions from the long-term mean state. Depending on the location of the peak warming of the sea surface temperature anomaly (SSTA), one usually distinguishes between Eastern Pacific (EP) and Central Pacific (CP) El Niño events. The EP events exhibit their largest SSTA warming in the eastern equatorial Pacific, while the CP events exhibit their largest warming westwards in the central equatorial Pacific. Although several studies have suggested the existence of a continuum between EP and CP events, e.g.,<sup>7,8</sup>, most studies of El Niño’s spatial diversity follow a splitting into two distinct groups. The shift of the location of the maximum SSTA during CP El Niños, compared to EP El Niños, towards the CP drives substantial shifts in atmospheric convection and circulation responses, which alter the location and intensity of temperature and precipitation impacts associated with El Niño around the globe<sup>8–16</sup>. In addition, since there is a strong correlation between the strength of an El Niño (e.g., Niño3.4 index, see below) and the longitude of the maximal warming<sup>8</sup>, EP events tend to be stronger and thus lead to more severe impacts around the globe.

For instance, large EP events typically lead to strongly increased precipitation along the coast of Ecuador and Northern Peru, resulting in massive floodings and landslides, while CP events only lead to dry conditions in these already dry areas and also to dryer conditions in the Peruvian Andes (see, e.g.,<sup>17,18</sup>). In India, particularly, CP events may lead to monsoon failures and thus to major droughts<sup>19</sup>. For more extensive discussions of the impacts of both El Niño types, we refer to, e.g.,<sup>10,11,16</sup>. These examples demonstrate that for mitigating the societal impact of an El Niño event by more targeted mitigation measures, it is crucial to have early operational forecasts not only for the event itself but also for the type of the event.

Currently, type forecasts based mainly on the warming pattern have quite limited lead times. For instance, Hendon et al.<sup>20</sup> found that the coupled ocean-atmosphere seasonal forecast model of

the Australian Bureau of Meteorology is limited to less than 1 season in predicting the SSTA pattern of EP and CP events. In a more recent and comprehensive study, Ren et al.<sup>21</sup> analyzed 6 operational climate models and found that only 2–3 can distinguish at 1 month lead time between CP and EP events. Zhang et al.<sup>22</sup> focused on hindcasts of the Climate Forecast System version 2 (CFSv2). They found that the skill of the CFSv2 model was comparable to the one reported by Ren et al.<sup>21</sup> and concluded that the CFSv2 model was broadly representative of the state-of-the-art forecast systems.

For comparison, without distinction between CP and EP events, the current forecasts in operation (which are hampered by the spring barrier) have a typical reliable lead time of about 6 months<sup>6,23</sup>. GCM forecasts with 12–24 months lead time are also possible<sup>24–26</sup> but with considerably less skill (see Method Section). Forecasts based on a climate network<sup>27–29</sup> approach have a lead time of about 1 year (see also Methods Section)<sup>30,31</sup>.

Since EP El Niños tend to be stronger than CP El Niños, forecasts of the El Niño strength can also be regarded as an indirect forecast for the type. Such forecasts of the El Niño strength are made, for instance, by several models of the North American Multi-Model Ensemble (NMME) with lead times up to 12 months (see Methods Section). To avoid forecast busts that sometimes afflict NMME-based objective forecasts and to provide more reliable El Niño strength forecasts<sup>32</sup>, the National Oceanic and Atmospheric Administration relies on subjective expert forecasts that are objectively translated<sup>33</sup> into probabilities that the strength of an El Niño (Niño3.4 index) will exceed given threshold values. Currently, these magnitude forecasts are not mapped operationally into explicit forecasts for the type of an event. The Peruvian multisector commission for the study of El Niño (ENFEN) provides operational forecasts for the temperatures in the Niño1 + 2 area located of the coast of Ecuador and Peru<sup>34</sup>. A warming in this area is called a coastal El Niño (“El Niño costero”) and tends to coincide with “global” EP El Niños. Thus, this forecast is highly related to an EP El Niño forecast. However, coastal El Niños can also be present without a global El Niño, as was the case during the devastating El Niño costero of 2017<sup>35</sup>.

<sup>1</sup>Potsdam Institute for Climate Impact Research (PIK), Member of the Leibniz Association, 14412 Potsdam, Germany. <sup>2</sup>Institut für Theoretische Physik, Justus-Liebig-Universität Giessen, D-35392 Giessen, Germany. ✉email: josef.ludescher@pik-potsdam.de

In the present study, we consider the period between 1950 and present, where reliable data on the El Niño events exist. We show that from the available SSTA data in the tropical Pacific, a precursor for CP and EP events can be obtained about 1 year before the peak of the event with high prediction skill. The type precursor does not forecast the onset of an El Niño event by itself, thus it is most useful when combined with other methods that forecast the onset of an El Niño event, irrespective of its type. When combined either with dynamical model forecasts in operation or the recently established climate network approach, one arrives at significantly better forecasts for the type of an El Niño event. Recently, in December 2022, the type precursor combined with the climate network approach forecasted the onset of an EP event in 2023<sup>36</sup>.

## RESULTS

### Classification of the El Niño types

To identify the types of the 23 El Niño events between 1950 and present (here, the El Niño events from 1986–1988 and 2014–2016 are counted as one event each), we have used 11 classification approaches<sup>9,10,37–45</sup>. Most of these approaches rely on compressing/projecting the diverse spatial SSTA patterns in the tropical Pacific into simple scalar numbers, i.e., indices. The choice of which geographical areas, times of the year, or physical quantities to regard and how to analyze the data leads to a large set of possible indices. Figure 1 summarizes the classification according to the 11 methods. For details, see Supplementary Note 1. For the majority of El Niño events, in particular the strong ones, there is a high consensus about the type irrespective of the approach. For the events in 1969/70 and 1986–1988, there is lacking consensus, so we keep them as unidentified. For more details, see Supplementary Note 1.

### Precursor for the type of the next El Niño event

Due to the mostly easterly winds of the Walker circulation, the climatological background state of the equatorial Pacific is characterized by a temperature gradient from the cold tongue in the east to the warm pool in the west. Accordingly, the simplest conceptual models of ENSO, for instance, the recharge-oscillator model developed by Jin<sup>46</sup>, divide the Pacific into two regions, the western Pacific and the EP. The models are able to describe the occurrence of the canonical EP events but not of CP events<sup>47</sup>.

Since CP El Niños are located in the CP, it appears natural to extend the two-region conceptual models by including the CP as a third region. This region is important for the development of

CP events since the zonal advective feedback is most effective here<sup>47,48</sup>. Such three-region models were developed by Fang and Mu<sup>47</sup> and Chen et al.<sup>49</sup> and indeed allow for the occurrence of both EP and CP events<sup>49</sup>. Within their model, Chen et al.<sup>49</sup> found that the zonal SST difference between the WP and CP influenced the frequency of CP events on decadal scales suggesting that the occurrence of CP events may be related to the zonal SST difference between the WP and CP. Here, we follow this idea but study the *interannual* fluctuations of the zonal temperature difference between the WP and CP.

To be specific, we consider the monthly zonal SSTA difference  $\Delta T_{WP-CP}$  between two equal-sized areas in the west Pacific (120E–165E, 5N–5S) and the CP (165E–150W, 5N–5S) (see Fig. 2). For the total area covering the central and western Pacific, we follow Fang and Mu<sup>47</sup>. Then, we divide the whole domain between 120E and 150W into two equal-sized areas. We would like to note that also Ashok et al.<sup>10</sup> used 165E as the western edge of the CP when defining the El Niño Modoki Index (EMI). Modifying the meridional width of the two areas or using an unequal partitioning as Fang and Mu<sup>47</sup> leads to little to no impact (see Supplementary Figs. 2–5). To account for the different effects of climate change in both regions, we use a trailing 30 year climatology, i.e., we calculate the temperature anomalies based only on the past of the considered point in time.

Figure 3 shows the difference  $\Delta T_{WP-CP}(t)$  between the mean SSTA in both areas, as a function of time  $t$  (maroon line), starting in 1950 and ending at present. The blue line is the Oceanic Niño Index (ONI), which is defined as the 3-month running-mean SSTA in the Niño3.4 region (see Fig. 2). The filled areas mark the El Niño events where the ONI is at least for 5 months greater or equal 0.5°C. The orange color stands for the 9 EP El Niño events, the violet color for the 12 CP events, obtained from our consensus classification. For the El Niño events starting in 1969 and the event starting in 1986 and ending in 1988, there is no consensus, so they are marked gray.

The figure shows that  $\Delta T_{WP-CP}(t)$  looks like a mirror image of the ONI, running through deep minima right at the peak of an El Niño event and reaching strong maxima in pronounced La Niña events. This is to be expected as El Niño episodes lead, e.g., to a warmer and La Niña episodes to a colder CP. However, a closer inspection reveals that in the last months of a year *preceding* an El Niño onset,  $\Delta T_{WP-CP}(t)$  tends to be positive when the upcoming event is an EP event and negative when it is a CP event. In the following, we will use this feature as a precursor for the type of an upcoming El Niño, with a lead time of about 1 year.

To be specific, we focus on the December values of  $\Delta T_{WP-CP}(t)$  for each year between 1950 and 2021. When a December value is

Method	51	53	57	58	63	65	68	69	72	76	77	79	82	86	87	91	94	97	02	04	06	09	14	15	18
Ashok 2007	E	E	C	C	C	C	C	E	E	E	C		E	E	E	C	C	E	C	C	E	C	E	E	
Feng 2020	E		E		E	E	C		E	E	C		E	E		C	C	E	C	C	E	C	E	E	
Kao 2009	E	C	C	C	C	C	C	C	E	E	C	C	E	C	C	C	E	C	C	C	E	C	C	E	C
Kim 2009	E		E		E	E		C	E	E			E		E	C	C	E	C	C					
Kug 2009	E		E		E	E	C		E	E	C		E	M	M	M	C	E	C	C	E	C	E	E	M
Larkin 2005	E		E		C	E	C	E	E	E	C	C	E	C	E	E	E	C	E	E					
Ren 2011	E	C	E	C	C	E	C	E	E	E	C		E	E	C	E	C	E	C	C	E	C			
Takahashi 11	E		C		C	C	C		E				E	M	C	C	C	E	C	C	C	C	C		M
Wiedermann 16		C	E	C	C	E	C	C	E	E	C	C	E	C	C	C	E	C	C	C	C	C	C	E	
Yeh 2009	E		E		E	E	C	E	E	E	C	E	E	E	E	E	C	E	C	C	E				M
Yu 2013	M	M	C		C	C	C	C	M	M	C		E	M	C	C	C	E	C	C	M	C			
Consensus	E	C	E	C	C	E	C	M	E	E	C	C	E	M	M	C	C	E	C	C	E	C	E	E	C

**Fig. 1 Classification of the type of El Niño events.** The table summarizes the classification according to 11 approaches. The numbers in the first row indicate the last two digits of the El Niño onset years. Eastern Pacific El Niños are marked 'E' and shown in orange. Central Pacific El Niños are marked 'C' and shown in blue. El Niño events marked by 'M' are not identified as pure EP or CP events, see Supplementary Note 1.

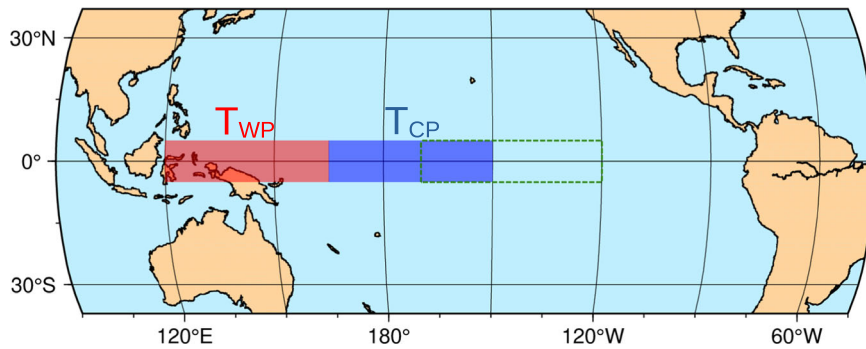


**Fig. 2** The areas of the regarded sea surface temperature anomalies (SSTA). The sign of the zonal difference  $\Delta T_{WP-CP}$  between the SSTA in the western equatorial Pacific and the SSTA in the central Pacific is predictive of the type of an upcoming El Niño event. The red area represents the western warm pool, the blue area nearly coincides with the Niño4 area, where CP El Niño events are centered. Varying the meridional width of the two areas or using an unequal partitioning as in ref. 47 leads to little to no impact (see Supplementary Figs. 2–5). The dashed green rectangle shows the Niño3.4 area.

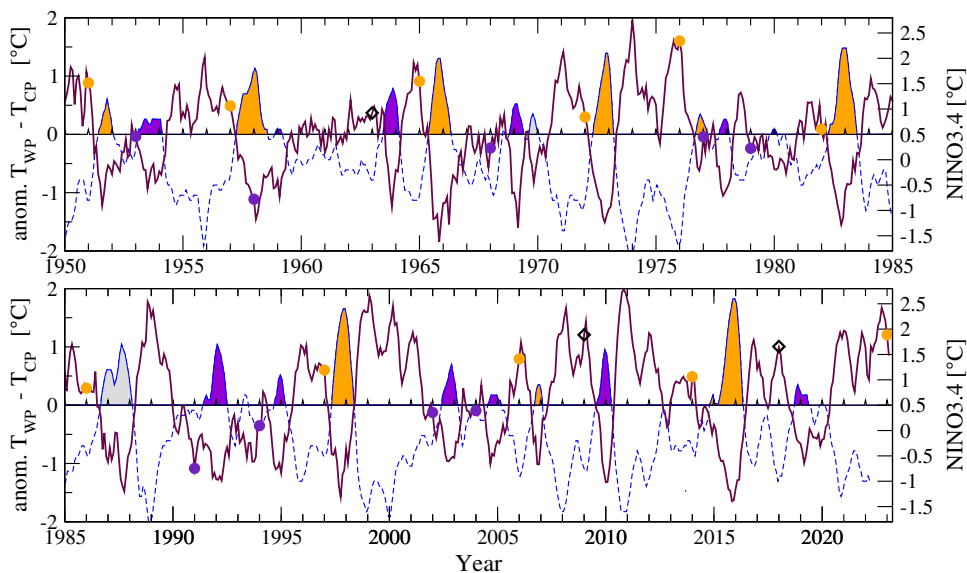


**Fig. 3** SSTA based forecasting scheme for the type of an upcoming El Niño event. The figure shows the anomaly of the monthly sea surface temperature difference between the equatorial western Pacific (120E–165E, 5N–5S) and central Pacific (165E–150W, 5N–5S) (left scale, maroon line) and the ONI (right scale, blue dashed line). The shaded areas highlight El Niño episodes, in orange EP El Niños and in violet CP El Niños according to the consensus (majority classification) from Fig. 1. The classification methods lead to a tie for the 1969/70 El Niño and the 1986–1988 multiyear El Niño (both in gray). Positive values of  $\Delta T_{WP-CP}(t)$  at the end of a calendar year serve as a precursor that an upcoming El Niño in the following year will be of EP type, while negative values serve as a precursor that it will be of CP type. Of the 21 El Niño type forecasts, 18 are correct: there are nine correct predictions for an EP type (orange circles), three false predictions where instead of an EP type, a CP type occurred (black diamonds), and nine correct predictions of a CP type (violet circles), resulting in a  $p$ -value below  $10^{-3}$ . In December 2022,  $\Delta T_{WP-CP}(t) = 1.21$  °C. Thus, the El Niño that started in 2023 will probably be an EP event, as forecasted in ref. 36. The type precursor does not forecast the onset of an El Niño event, thus it is most useful when combined with other methods that forecast the onset of an El Niño event, irrespective of its type. Such onset forecasting methods are available even before the spring barrier, see, e.g., refs. 30,67.

positive, we expect that an upcoming El Niño will be an EP event, otherwise a CP event. Figure 3 shows that the type forecast based on this precursor is correct for all nine EP El Niños. There are three “false alarms”, in 1962, 2008, and 2017, where an EP type is forecasted, but a CP type is observed in the following year. In contrast, all 9 CP type forecasts were correct. Accordingly, when  $\Delta T_{WP-CP}(t)$  is negative in December, we can be highly certain that a potentially upcoming event will be a CP event, i.e., a possibly disastrous EP event in the following year can be excluded with high probability. Otherwise, when  $\Delta T_{WP-CP}(t)$  is positive in December, an upcoming El Niño will be an EP event with 75 percent probability. In December 2022,  $\Delta T_{WP-CP}(t) = 1.21$  °C. Thus, the El Niño that started in 2023 will probably be an EP event.

In total, 18 out of 21 events were correctly forecasted. When random guessing with the past occurrence probabilities of EP and CP El Niño events, the  $p$ -value for correctly predicting 18 of 21 events is  $p = 9.1 \times 10^{-4}$ , i.e., the predictions by our precursor are highly significant. For the calculation of the  $p$  value, see the Methods Section.

Our choice of December as the calendar month to evaluate  $\Delta T_{WP-CP}(t)$  is motivated by the fact that the climate network-based approach discussed below provides its El Niño forecasts by the end of the calendar year. Additionally, ENSO is phase-locked to the seasonal cycle and El Niños and La Niñas tend to peak around December. The same prediction skill is obtained when, instead of December(D), the 3-month averages NDJ and DJF are considered. For a more extensive discussion, see Supplementary Figs. 6, 7.

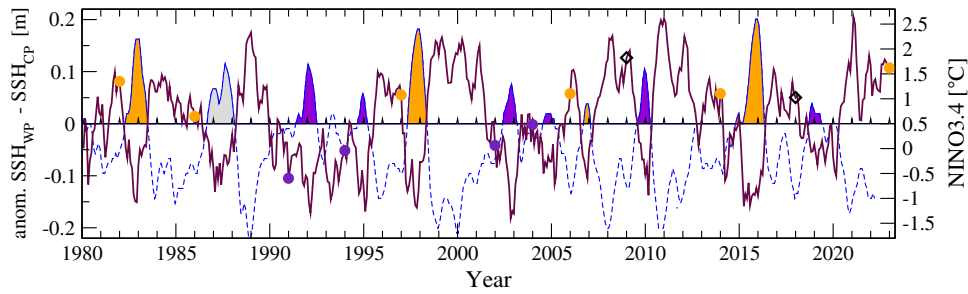


**Fig. 4 SSHA based forecasting scheme for the type of an El Niño event.** Same as Fig. 3 but for the anomaly of the monthly sea surface height (SSH) difference between west Pacific and central Pacific as predictor for the type of an El Niño. Forecasting based on SSHA leads to the same forecasts as that based on SSTA.

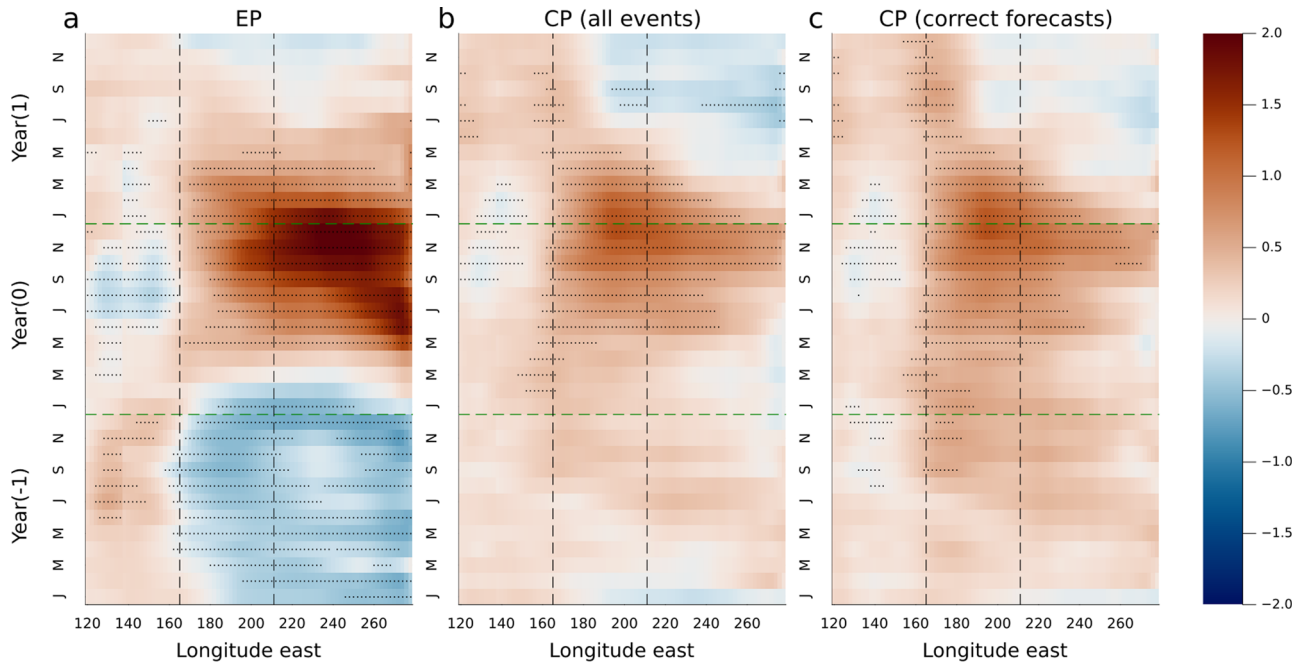


**Fig. 5 Composite evolution of equatorial SSTAs for different subsets of El Niños.** **a** all EP El Niños, **(b)** all CP El Niños, and **(c)** the CP El Niños that were correctly forecasted by  $\Delta T_{WP-CP}$ . The longitude-time diagrams show the SSTA in °C averaged between 5N and 5S. The figure shows that in the second half of the year before an EP event, there is a warming in the western Pacific while the central Pacific is significantly colder. In the year before a CP El Niño, there is a mild warming in the central Pacific, which later expands eastward. Subfigure **(b)** includes the 3 El Niños that were incorrectly forecasted as EP events. When only correctly forecasted CP events are considered **(c)**, the warm anomalies in the center Pacific are more pronounced and cold anomalies are present in the western Pacific in the year before the onset. The figures confirm that  $\Delta T_{WP-CP}$ , which aggregates these patterns, is predictive of the type of an El Niño in the calendar year before the onset.

Apart from the zonal SSTA difference, the zonal sea surface height anomaly (SSHA) difference and the zonal surface air temperature anomaly difference are strongly related to the Walker circulation and its fluctuations. Figure 4 shows the difference of the monthly SSHAs between 1980 and present. The figure shows that the SSHA is highly correlated with the SSTA and leads to the same forecasts. As we show in Supplementary Fig. 8, the surface air temperature anomalies are also highly correlated with the SSTA and lead to the same forecasting performance. We like to note that our findings are consistent with Ashok et al.<sup>10</sup>, where correlation maps for the EMI with the SSHA and SSTA in the tropical Pacific have been calculated.

For a better understanding of our findings, we analyse the spatial and temporal development of the SSTA. Figure 5 shows the evolution of the equatorial Pacific SSTAs starting in the year before an El Niño onset and ending in the year after the onset. The longitude-time diagrams show the SSTA in °C averaged between 5N and 5S. Figure 5a and b show the composites over all EP and CP events as classified by our consensus classification shown in

Fig. 1. Stippling shows significant differences at 90% level to all not regarded years and was obtained from a two-tailed student's t-test.

In the second half of the year, before an EP El Niño starts, significantly warmer SSTAs are present in the western Pacific and significantly colder SSTAs in the central Pacific, which are characteristic for La Niña conditions. The positive SSTAs in the west can indicate an anomalously deep thermocline here and, thus, positive warm water volume anomalies. This is confirmed by the positive sea surface height anomalies (SSHA), which are highly correlated with the thermocline depth. In the year before the onset of an EP El Niño, there are pronounced positive SSH anomalies in the western Pacific, which shows that the thermocline is indeed deeper here (see Supplementary Fig. 9).

In the year before the onset of a CP El Niño, there is already a mild warming in the central Pacific, which expands eastwards in the following year and develops into a CP El Niño, see Fig. 5b. For CP El Niños, the anomalies in the year before the El Niño onset are not statistically significant at a data point level since the figure also

contains the years where our predictor incorrectly forecasted an EP El Niño. Excluding these years leads to statistically significant positive anomalies in the central Pacific and negative anomalies in the western Pacific, see Fig. 5c. Thus, Figure 5 confirms that a positive sign of  $\Delta T_{WP-CP}$  is a precursor for EP El Niño events and a negative sign is a precursor for CP events. The SSTA differences present in the year before the El Niño onset are significant, partially even at a data point level (see Supplementary Fig. 10).

Interestingly, the precursor predicted the onset of CP events accurately, while only 75% of the EP predictions turned out to be correct. This difference in the EP and CP predictability can result from stochastic processes, most likely westerly wind events (WWE) that typically start in boreal spring and are highly relevant for triggering El Niño events. WWEs can be regarded as state dependent noise, where warmer sea surface temperatures in the western and central Pacific favor more WWEs<sup>5</sup>. It has been noticed by Jadhav et al.<sup>50</sup> that stronger boreal spring through summer WWEs, with relatively stronger ocean preconditioning (e.g., large SSHA in the west<sup>51</sup>), can lead to EP events, while weaker ocean preconditioning (small SSHA in the west<sup>51</sup>) and weaker WWE can generate CP events. For similar arguments, see, e.g.,<sup>52–54</sup>.

This argument is supported by Fig. 5 and Supplementary Fig. 9, which show that before an EP El Niño, the western Pacific is warmer and has a deeper thermocline, i.e., it is in a charged state. With sufficiently strong WWEs in the following boreal spring, the system likely develops into an EP El Niño. However, when the WWE activity is weaker, the upcoming El Niño develops likely in a CP event. In contrast, before the correctly type forecasted CP El Niños, the western Pacific is slightly colder, and the thermocline is somewhat shallower than the climatological average, i.e., it is not in a charged state. In this case, WWEs can only trigger CP events. This explains why we do not see incorrect CP forecasts.

Supplementary Fig. 9 also shows the composite of the SSHA evolution for the 2009 and 2018 El Niños. The type of both events was forecasted as an EP, but they turned out to be CP events. The figure shows that the SSHA is positive in the western Pacific the year before the onset, as it is before EP events, i.e., a charged state is present. However, in both onset years, there were only weaker westerly wind anomalies, in particular in the first half of the year, see Supplementary Fig. 11. The same holds for 1963. Thus, in all three cases, favorable conditions for an EP event were present in the year before the onset, but since WWEs are at least partially stochastic, the insufficient WWE activity probably led to the CP events.

### Forecasting El Niño events and their type

The type precursor does not forecast the onset of an El Niño event by itself, thus it is most useful when combined with other methods that forecast the onset of an El Niño event, irrespective of its type (see, e.g., refs. 55–70). Some of these methods are available even before the spring predictability barrier, see, e.g., refs. 30,67. For simplicity, we discuss here two kinds of forecast:

**Dynamical models.** Coupled general circulation models (GCM) are initialized by observations and directly simulate the further development of physical quantities like the SSTA. When the predicted development of the ONI, i.e., the SSTA in the Niño3.4 region, also referred to as Niño3.4 index, satisfies the definition of an El Niño, the models predict the onset of an El Niño event. Since the predictions of these models are hampered by the spring barrier, the typical reliable lead time is about 6 months<sup>6,23</sup>. For longer lead times, the prediction skill of the models decreases considerably. For instance, 4 models of the North American Multi-Model Ensemble (see Methods Section) provide forecasts with 11 months lead time by forecasting the SST in the Niño3.4 area. We regard reforecasts starting on 1 January. For evaluating the skill of the four ensemble means, we assume that an ensemble

**Table 1.** Contingency table showing the skill of the forecasting methods in predicting the type of an El Niño event.

Observed outcome	direct		$\Delta T_{WP-CP}$		$\Delta T_{WP-CP}$		$\Delta T_{WP-CP}$	
	GCM		GCM		network v(i)		network v(ii)	
	1 month		11 months		11 months		11 months	
	EP	CP	EP	CP	EP	CP	EP	CP
EP	49	31	38	0	67	0	67	0
CP	41	50	15	38	11	70	11	100
Other	10	19	46	63	22	30	22	0

Tabulated are the percentages of events that are observed to occur, given an approach has forecasted an EP or CP El Niño event. “Other” outcomes are neutral or La Niña events. The first approach shows the results of a direct forecast of El Niño and its type based on the SST warming pattern at a 1 month lead time, as reported by Ren et al.<sup>21</sup>. The following approaches combine the type forecast based on  $\Delta T_{WP-CP}$  with 11 months lead time onset forecasts of models of the North American Multi-Model ensemble and the two versions of the climate network, respectively. Sums can deviate from 100% since the numbers are rounded to full percentages.

predicts the onset of an El Niño when the forecasted December temperature anomaly is equal or above 0.5 °C. At 11 months lead time, 53% of the El Niño onset “alarms” turned out correct. When combined with our type precursor, 38% of the EP El Niño forecasts are correct, while 15% lead to a CP El Niño and 46% to a false alarm, see Table 1. Similarly, 37.5% of the CP El Niño forecasts are correct, while 62.5% lead to a false alarm.

A systematical study of the performance of direct El Niño type prediction relying on the SSTA warming patterns has been done by Ren et al.<sup>21</sup>, who focused on six operational GCMs. All models were initialized in November. Then the predicted temporal and spatial distribution of the SSTA in December, January and February is used to forecast whether an El Niño event will come and whether it will be an EP or CP event. Despite the very short lead time, only about every second EP or CP event was correctly forecasted, see Table 1. Combining GCM El Niño onset forecasts (irrespective of the type) with type forecasts based on the sign of  $\Delta T_{WP-CP}(t)$  would lead to much improved type forecasts. The limited skill in distinguishing between EP and CP events might be due to the GCMs’ biases in simulating the background mean state<sup>71–74</sup>.

**Climate network approach.** The climate network approach<sup>30,31</sup> (at the time of publication based on data between 1950 and 2011) is described in the Methods Section. Here we consider, as in Fig. 3, the period between 1950 and 2022. In its original version (i) (see Fig. 6a and Supplementary Fig. 12), the approach yields 20 alarms in the year before the onset of an El Niño event; 15 forecasts are correct, including 6 of the 8 largest El Niño events (see Supplementary Fig. 12). Accordingly, 75% of the alarms are correct.

For the target years 2012–2023, i.e., out of-sample into the future, the algorithm provided 12 forecasts, 11 of which turned out to be correct. For instance, it correctly warned of the onset of El Niños in 2014<sup>31</sup> and 2023<sup>36</sup>. The total *p*-value of the predictions (including learning, hindcasting, and forecasting phase) calculated from random guessing with the climatological El Niño onset probability (about 1/3 per year) is  $p = 1.3 \times 10^{-7}$ .

Combining this approach with our type precursor shown in Fig. 3, the method correctly forecasts 6 EP events (among them the four largest ones) and 7 CP events. When the climate network approach sounded a correct alarm, then also the type of the event

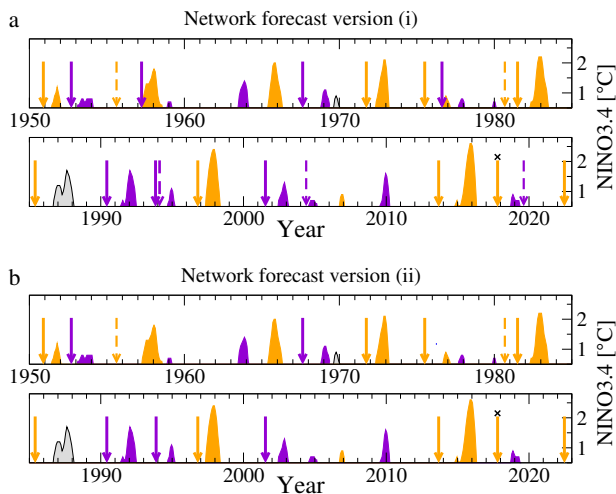


**Fig. 6 Summary of the combined prediction scheme.** Shaded areas mark the El Niño events: EP (orange), CP (violet), not classified (gray). Alarms of the network-based method (version (i) in (a) and version (ii) in (b)) are combined with the forecast based on the temperature anomaly difference  $\Delta T_{WP-CP}(t)$  (Fig. 3) and shown as arrows in the color of the forecasted El Niño type. False alarms of the network-based method are shown as dashed arrows. The single incorrect forecast of the type (2017) is marked by an 'x'. For better visibility, we have doubled the height of the 2 smallest CP events, starting in 1958 and 1979. In 2022, both versions forecasted for 2023 the onset of an EP El Niño, which at present (October 2023) is very likely to occur.

was correctly forecasted, with one exception in 2017. Accordingly, when an EP event was forecasted, the forecast was about 67% correct, in 11% of the cases a CP event was observed, and in 22% of the cases an El Niño did not occur. (The correct alarm in 1985 before the non-identified event starting in 1986 was not counted.) When a CP event was predicted, 70% of the predicted events were CP events and 30% no El Niño events.

In its more restricted version (ii) (see Fig. 6b and Supplementary Fig. 13), the climate network approach sounds 15 alarms, 13 of which are correct alarms and two false alarms. Compared with version (i), the two correct alarms for the smallest El Niño events (1958/59 and 1977/78, both CP events) are missing. Now 86.7% of the alarms are correct and for all correct alarms, except that one in 2017, the type of the El Niño is correctly forecasted. As in version (i), 67% of the predicted EP events were EP events, 11% were CP events, and 22% percent no events. But now, each prediction of a CP event was correct.

Table 1 compares the performance of the two versions of the climate network approach with the performance of operational GCMs when they directly predict the type of an El Niño and when our type predictor is combined with GCM El Niño onset forecasts (irrespective of the type). The table shows that our approach, which is based solely on the zonal SSTA difference between the equatorial western and central Pacific, when combined with the climate network approach, considerably outperforms the direct GCM approach, even though its lead time is one order of magnitude longer. Also, when the type predictor is combined with the climate network, it delivers more skillful forecasts at the same 11 months lead time than when it is combined with GCM onset forecasts.

We would like to note that since the type and magnitude of an El Niño event are closely related, our type forecast does also represent an indirect forecast for the magnitude of an event. In the period between 1950 and 2022, the average of the maximal ONI value during EP events was  $1.79 \pm 0.64$  °C, while during CP events, it was  $1.05 \pm 0.38$  °C. Thus, our combined approach can

warn of EP El Niños, which have the potential to become very strong and lead to more extreme events around the globe.

## DISCUSSION

In summary, by studying the zonal SSTA difference between the equatorial western and central Pacific, we arrived at a precursor which allows to predict the type of an El Niño event well before the spring barrier with a high accuracy. The approach relies only on the sign of the zonal SSTA difference at the end of a year. When it is positive, an El Niño event arising in the following year will probably be an EP event, otherwise a CP event. Interestingly, the precursor predicted the onset of CP events accurately, while only 75% of the EP predictions turned out to be correct.

We attribute this difference in predictability to stochastic processes, most likely WWEs that typically start in boreal spring and are highly relevant for triggering El Niño events. WWEs can be regarded as state dependent noise, where warmer sea surface temperatures in the WP and CP favor more WWEs<sup>5</sup>. It has been noticed by Jadhav et al.<sup>50</sup> that stronger boreal spring through summer WWEs, with relatively stronger ocean preconditioning (e.g., large SSHA in the west), can lead to EP events, while weaker ocean preconditioning (small SSHA in the west) and weaker WWEs can generate CP events. For similar arguments, see, e.g.,<sup>52–54</sup>.

Based on this, we interpret the difference in EP/CP predictability as follows: When the zonal difference of the SSTA (Fig. 3) or the SSHA (Fig. 4) is positive at the end of a year and sufficiently strong WWEs occur in boreal spring in the following year, an upcoming event will most probably be an EP event, but for weaker WWEs, a CP event may occur with high probability. This can explain the 25% incorrect EP forecasts. On the other hand, when the zonal difference is negative, the WWEs can only trigger CP events, and this may explain why we do not see incorrect CP forecasts.

As we have shown in detail, this interpretation is supported by our analysis of the SSHAs and SSTAs. At the end of the year before the onset of an EP El Niño, both quantities show positive anomalies in the western Pacific, i.e., the system is in a charged state. In contrast, before correctly forecasted CP events, both quantities are slightly negative, i.e., the system is not in a charged state. Additionally, in the years in which the incorrect EP forecasts were made, the SSHA in the western Pacific was positive, however, during the following onset years, only weak westerly wind activities were present and the El Niños developed into CP events.

By construction, the type precursor can be combined with any method that forecasts the onset of an El Niño event. However, GCM forecasts are hampered by the spring barrier. For instance, at a lead time of 11 months, only 53% of the regarded single-model ensemble forecasts of an El Niño onset were correct. In contrast, 75% of the El Niño onset forecasts (irrespective of the type) of the climate network approach were correct at lead times of at least 11 months.

To take full advantage of the type predictor, we have combined it with the climate network approach. The climate network sounds an alarm when its mean link strength exceeds a fixed threshold and the ONI remains below 0.5 until the end of the year. In this case, the onset of an El Niño event is forecasted for the next calendar year. From the perspective of predicting the major disastrous events, whose probability might increase in a warming climate<sup>75</sup>, the combined approach was quite successful. In the last 7 decades, it forecasted the 4 largest El Niño events. In December 2022, the combined approach forecasted the onset of an El Niño event with 80% probability and, in case of onset, an EP El Niño with 86% probability, putting Ecuador and Northern Peru at increased risk of extreme rainfall. We would like to note that the here presented combined approach can be complemented by an information entropy-based approach<sup>67</sup>, which provides direct forecasts for the magnitude of upcoming El Niño events before the spring barrier. For 2023, this method forecasted the onset of a

moderate-to-strong El Niño with a magnitude of  $1.49 \pm 0.37^\circ\text{C}$ <sup>36</sup>, which is consistent with the here forecasted onset of an EP El Niño.

Since our El Niño type prediction approach is based on temperature anomalies that are obtained from trailing climatologies, we believe that it remains valid also under the upcoming climate change conditions. Should the El Niño Southern Oscillation shift at some point into a different regime, where its general dynamics changes, then the approach should be reassessed. We hope that the approach will enable early and more targeted mitigation methods, either together with the climate network approach discussed here or with any other early forecasting approach, and thus help prevent or at least mitigate humanitarian disasters as consequences of El Niño related extreme weather impacts.

## METHODS

### North American Multi-Model Ensemble (NMME)

Four models of the NMME (CanCM4i, GEM5\_NEMO, GFDL\_SPEAR and NCAR\_CCSM4) provide forecasts with 11 months lead time. These dynamical models forecast globally a range of physical quantities like SSTs, in particular, the SSTs in the Niño3.4 area. We regarded reforecasts starting on 1 January. For evaluating the forecasts skill of the 4 ensemble means, we assume that an ensemble predicts the onset of an El Niño when the forecasted December temperature anomaly is equal or above  $0.5^\circ\text{C}$ . Since the absolute mean temperatures vary between models, we calculate the anomalies based on each model's mean December temperature over the full period. CanCM4i and NCAR\_CCSM4 start their reforecast in 1982 and the other models in 1991. In total, we have 36 El Niño onset “alarms” from the individual ensemble mean forecasts of the 4 models, 19 of which turned out correct, i.e., 53% of the onset alarms are correct. For instance, all 4 models correctly forecasted the onset of the 1997/98 El Niño, but 3 out of 4 models gave a false alarm in 2017. The GCM El Niño onset forecast is then combined with the observation-based  $\Delta T_{\text{WP-CP}}$  type forecast shown in Fig. 3. As for the climate network, the correct alarms before the non-identified El Niño event starting in 1986 were not counted.

### Climate network approach

The approach exploits the observation that a large-scale cooperative mode linking the “El Niño basin” (i.e., the equatorial Pacific corridor) and the rest of the tropical Pacific (see Supplementary Fig. 14 and refs. <sup>30,76</sup>) builds up in the calendar year before an El Niño event. The emerging cooperativity is derived from the time evolution of the teleconnections (“links”) between the surface air temperature anomalies (SATA) at the grid points (“nodes”) inside and outside of the El Niño basin. The strengths of these links at a given time  $t$  are derived from the values of the respective cross-correlations for which we consider time lags between 0 and 200 days. We determine, for each time  $t$ , the maximum, the mean, and the standard deviation around the mean of the absolute value of the cross-correlation function and define the link strength  $S_{ij}(t)$  as the difference between the maximum and the mean value, divided by the standard deviation. Accordingly,  $S_{ij}$  describes the link strength relative to the underlying background noise (signal-to-noise ratio) and thus quantifies the dynamical teleconnections between nodes  $i$  and  $j$ . To obtain the mean strength  $S(t)$  of the dynamical teleconnections in the climate network, we average over all individual link strengths (for more details, see Supplementary Note 2 and <sup>30,76</sup>). The mean link strength  $S(t)$  in the network usually rises in the year before an El Niño event starts and drops with the onset of the event. This feature serves as a precursor for the event.

The algorithm<sup>30</sup> involves as only fit parameter a decision threshold  $\Theta$ , which has been fixed in<sup>30</sup> during a learning phase between 1950 and 1980, and tested during a hindcasting phase between 1981 and 2011. Accordingly, the operational algorithm<sup>30</sup> has no free fit parameters. In its original version (i), the algorithm gives an alarm and predicts an El Niño inception in the following year whenever  $S$  crosses  $\Theta$  from below while the most recent ONI is below  $0.5^\circ\text{C}$ . This version aims at providing an El Niño warning as early as possible. For the target years 2012 - 2023, the algorithm provided 12 forecasts, out-of-sample into the future, 11 of which were correct. In the modified version (ii), the algorithm considers only those alarms for which the ONI remains below 0.5 for the rest of the calendar year. This way, version (ii) neglects not only alarms during an El Niño episode but also all alarms preceding the potential onset of an El Niño episode, where the ONI value  $\geq 0.5^\circ\text{C}$  at the end of the calendar year. Since  $\Delta T_{\text{WP-CP}}$  is evaluated at the end of the calendar year, waiting for the additional information about the development of the ONI does not lead to a delay when forecasting the onset *and* type of an El Niño.

### Calculating the $p$ -value of the type forecasts

In a series (configuration) of  $N$  type forecasts, we have  $E_t$  correct (true) EP type forecasts,  $E_m$  missed EP events, i.e., a CP event was forecasted, but an EP event turned out,  $C_t$  correct CP type forecasts and  $C_m$  missed CP type events. To obtain the statistical significance of this series, one has to determine the probability  $w_i$  that a configuration with the same total number of correct forecasts  $E_t + C_t$  can be obtained by randomly guessing. In addition, one has to consider all configurations  $K_1, K_2, \dots, K_s$  with an equal or higher number of total correct forecasts and determine the corresponding probabilities  $w_1, w_2, \dots, w_s$ . Then the probability  $p$  ( $p$ -value), that by randomly guessing the same or better forecasts can be obtained, is given by

$$p = \sum_{i=0}^s w_i. \quad (1)$$

Our null hypothesis is that the given forecast configuration can be obtained by randomly guessing with the climatological El Niño type probabilities. Of the 21 El Niño events classified in Fig. 1, nine are EP events, thus the probability of an EP type given an El Niño (of any type) is present, is  $q = 9/21$ ; correspondingly, for a CP type  $q_C = 1 - q = 12/21$ . In the simplest case, when all type forecasts are correct, there is only one configuration to consider and the  $p$  value is  $w = q^9(1-q)^{12}$ . More generally, for 9 EP and 12 CP events, the probability of a configuration is given by,

$$w = \binom{9}{E_t} \binom{12}{C_t} q^{E_t} (1-q)^{C_t} q^{E_m} (1-q)^{C_m}, \quad (2)$$

with the quantities as defined above. For example, 9 choose  $E_t$  is the number of ways (permutations) to rearrange  $E_t$  forecast out of 9 EP El Niños.

Since there are only 2 El Niño types and two possible outcomes (correct or false forecast), we have by definition that  $E_t + E_m = 9$  and  $C_t + C_m = 12$ . In the case considered here, there are 18 correct type forecasts and three false type forecasts. There are, in total, ten configurations that are equal or better:  $E_m = C_m = 0, E_m = 1$  and  $C_m = 0, E_m = 0$  and  $C_m = 1, E_m = 1$  and  $C_m = 1, E_m = 2$  and  $C_m = 0, E_m = 0$  and  $C_m = 2, E_m = 2$  and  $C_m = 1, E_m = 1$  and  $C_m = 2, E_m = 3$  and  $C_m = 0, E_m = 0$  and  $C_m = 3$ . Inserting these configurations into Eq. (2) and summing up the probabilities yields  $p = 9.132 \times 10^{-4}$ . Should the El Niño in 2023 turn out to be an EP El Niño as forecasted<sup>36</sup>, the corresponding calculation for 19 correct type forecasts out of 22 forecasts yields  $p = 4.665 \times 10^{-4}$ .

## DATA AVAILABILITY

All data used in this study are publicly available. The monthly sea surface temperatures were obtained from the National Oceanic and Atmospheric Administration (NOAA) Extended Reconstructed Sea Surface Temperature version 5 (ERSSTv5)<sup>77</sup> downloaded from <https://psl.noaa.gov/data/gridded/data.noaa.ersst.v5.html>. The daily surface air temperature (SAT) data (1948-present) for the calculation of the mean link strength  $S(t)$  of the network were obtained from the National Centers for Environmental Prediction/ National Center for Atmospheric Research (NCEP/NCAR) Reanalysis I project<sup>78</sup> downloaded from <https://www.psl.noaa.gov/data/gridded/data.ncep.reanalysis.html>. For the sea surface height (SSH), we used the monthly NCEP Global Ocean Data Assimilation System (GODAS)<sup>79</sup> data set downloaded from <http://apdrc.soest.hawaii.edu/erddap/index.html>. We downloaded the reforecasts of the North American Multi-Model Ensemble (NMME)<sup>80</sup> from <https://ftp.cpc.ncep.noaa.gov/NMME/ENSO/>.

## CODE AVAILABILITY

The codes used to produce these results are available from the corresponding author upon reasonable request.

Received: 14 May 2023; Accepted: 3 November 2023;

Published online: 22 November 2023

## REFERENCES

- Clarke, A. J. *An Introduction to the Dynamics of El Niño and the Southern Oscillation* (Elsevier, 2008).
- Sarachik, E. S. & Cane, M. A. *The El Niño-Southern Oscillation Phenomenon* (Cambridge Univ. Press, 2010).
- Dijkstra, H. A. *Nonlinear Physical Oceanography: A Dynamical Systems Approach to the Large-Scale Ocean Circulation and El Niño* (Springer, 2005).
- Wang, C. et al. El Niño and Southern Oscillation (ENSO): A Review, in *Coral Reefs of the Eastern Tropical Pacific* (eds. Glynn, P., Manzello, D., Enochs, I.) 85–106 (Coral Reefs of the World vol 8, Springer, 2017).
- Timmermann, A. et al. El Niño-Southern Oscillation complexity. *Nature* **559**, 535–545 (2018).
- McPhaden, M. J., Santoso, A. & Cai, W. (eds.) *El Niño Southern Oscillation in a Changing Climate* (John Wiley & Sons, 2020).
- Johnson, N. C. How many ENSO flavors can we distinguish? *J. Clim.* **26**, 4816–4827 (2013).
- Capotondi, A. et al. Understanding ENSO diversity. *Bull. Am. Meteorol. Soc.* **96**, 921–938 (2015).
- Larkin, N. K. & Harrison, D. E. Global seasonal temperature and precipitation anomalies during El Niño autumn and winter. *Geophys. Res. Lett.* **32**, L16705 (2005).
- Ashok, K., Behera, S. K., Rao, S. S., Weng, H. & Yamagata, T. El Niño Modoki and its possible teleconnection. *J. Geophys. Res.: Oceans* **112**, C11007 (2007).
- Weng, H., Ashok, K., Behera, S. K., Rao, S. A. & Yamagata, T. Impacts of recent El Niño on Modoki dry/wet conditions in the Pacific rim during boreal summer. *Clim. Dyn.* **29**, 113–129 (2007).
- Wang, G. & Hendon, H. H. Sensitivity of Australian Rainfall to Inter-El Niño Variations. *J. Clim.* **20**, 4211–4226 (2007).
- Taschetto, A. S. & England, M. H. El Niño Modoki Impacts on Australian Rainfall. *J. Clim.* **22**, 3167–3174 (2009).
- Frauen, C., Dommenges, D., Tyrrell, N., Rezny, M. & Wales, S. Analysis of the nonlinearity of El Niño–Southern oscillation teleconnections. *J. Clim.* **27**, 6225–6244 (2014).
- Freund, M. B. et al. Higher frequency of Central Pacific El Niño events in recent decades relative to past centuries. *Nat. Geosci.* **12**, 450–455 (2019).
- Wiedermann, M., Siegmund, J. F., Donges, J. F. & Donner, R. V. Differential imprints of distinct ENSO flavors in global patterns of very low and high seasonal precipitation. *Front. Clim.* **3**, 618548 (2021).
- Lagos, P., Silva, Y., Nickl, E. & Mosquera, K. El Niño related precipitation variability in Peru. *Adv. Geosci.* **14**, 231–237 (2008).
- Bazo, J., Lorenzo, M. D. L. N. & Porfirio da Rocha, R. Relationship between monthly rainfall in NW Peru and tropical sea surface temperature. *Adv. Meteorol.* **2013**, 152875 (2013).
- Kumar, K. K., Rajagopalan, B., Hoerling, M., Bates, G. & Cane, M. Unraveling the mystery of Indian monsoon failure during El Niño. *Science* **314**, 115–119 (2006).
- Hendon, H. H., Lim, E., Wang, G., Alves, O. & Hudson, D. Prospects for predicting two flavors of El Niño. *Geophys. Res. Lett.* **36**, L19713 (2009).
- Ren, H. L. et al. Seasonal predictability of winter ENSO types in operational dynamical model predictions. *Clim. Dyn.* **52**, 3869–3890 (2019).
- Zhang, T., Hoerling, M. P., Hoell, A., Perlwitz, J. & Eischeid, J. Confirmation for and predictability of distinct US Impacts of El Niño flavors. *J. Clim.* **33**, 5971–5991 (2020).
- Barnston, A. G., Tippett, M. K., L’Heureux, M. L., Li, S. & DeWitt, D. G. Skill of real-time seasonal ENSO model predictions during 2002–11: Is our capability increasing? *Bull. Am. Meteorol. Soc.* **93**, 631–651 (2012).
- Barnston, A. G., Tippett, M. K., Ranganathan, M. & L’Heureux, M. L. Deterministic skill of ENSO predictions from the North American Multimodel Ensemble. *Clim. Dyn.* **53**, 7215–7234 (2019).
- Tippett, M. K., Ranganathan, M., L’Heureux, M. L., Barnston, A. G. & DelSole, T. Assessing probabilistic predictions of ENSO phase and intensity from the North American Multimodel Ensemble. *Clim. Dyn.* **53**, 7497–7518 (2019).
- Weisheimer, A. et al. Variability of ENSO forecast skill in 2-year global reforecasts over the 20th century. *Geophys. Res. Lett.* **49**, e2022GL097885 (2022).
- Tsonis, A. A., Swanson, K. L. & Roebber, P. J. What do networks have to do with climate? *Bull. Am. Meteorol. Soc.* **87**, 585–595 (2006).
- Fan, J. et al. Statistical physics approaches to the complex Earth system. *Phys. Rep.* **896**, 1–84 (2020).
- Ludescher, J. et al. Network-based forecasting of climate phenomena. *Proc. Natl. Acad. Sci. USA* **118**, e1922872118 (2021).
- Ludescher, J. et al. Improved El Niño forecasting by cooperativity detection. *Proc. Natl. Acad. Sci. USA* **110**, 11742–11745 (2013).
- Ludescher, J. et al. Very early warning of next El Niño. *Proc. Natl. Acad. Sci. USA* **111**, 2064–2066 (2014).
- Climate Prediction Center - El Niño Southern Oscillation, [https://www.cpc.ncep.noaa.gov/products/analysis\\_monitoring/enso\\_advisory/strengths/index.php](https://www.cpc.ncep.noaa.gov/products/analysis_monitoring/enso_advisory/strengths/index.php).
- L’Heureux, M. L. et al. Strength Outlooks for the El Niño-Southern Oscillation. *Weather Forecast.* **34**, 165–175 (2019).
- Informes y publicaciones—Instituto del Mar del Perú, <https://www.gob.pe/institucion/imarpe/informes-publicaciones>.
- Rodríguez-Morata, C., Díaz, H. F., Ballesteros-Canovas, J. A., Rohrer, M. & Stoffel, M. The anomalous 2017 coastal El Niño event in Peru. *Clim. Dyn.* **52**, 5605–5622 (2019).
- Ludescher, J., Meng, J., Fan, J., Bunde, A. & Schellnhuber, H. J. Very early warning of a moderate-to-strong El Niño in 2023. Preprint at <https://arxiv.org/abs/2301.10763> (2023).
- Kao, H. Y. & Yu, J. Y. Contrasting eastern-Pacific and central-Pacific types of ENSO. *J. Clim.* **22**, 615–632 (2009).
- Kim, H. M., Webster, P. J. & Curry, J. A. Impact of shifting patterns of Pacific Ocean warming on North Atlantic tropical cyclones. *Science* **325**, 77–80 (2009).
- Kug, J. S., Jin, F. F. & An, S. I. Two types of El Niño events: cold tongue El Niño and warm pool El Niño. *J. Clim.* **22**, 1499–1515 (2009).
- Yeh, S. W. et al. El Niño in a changing climate. *Nature* **461**, 511–514 (2009).
- Ren, H. L. & Jin, F. F. Niño indices for two types of ENSO. *Geophys. Res. Lett.* **38**, L04704 (2011).
- Takahashi, K., Montecinos, A., Goubanova, K. & Dewitte, B. ENSO regimes: Reinterpreting the canonical and Modoki El Niño. *Geophys. Res. Lett.* **38**, L10704 (2011).
- Yu, J. Y. & Kim, S. T. Identifying the types of major El Niño events since 1870. *Int. J. Climatol.* **33**, 2105–2112 (2013).
- Wiedermann, M., Radebach, A., Donges, J. F., Kurths, J. & Donner, R. V. A climate network-based index to discriminate different types of El Niño and La Niña. *Geophys. Res. Lett.* **43**, 7176–7185 (2016).
- Feng, J., Lian, T., Ying, J., Li, J. & Li, G. Do CMIP5 models show El Niño diversity? *J. Clim.* **33**, 1619–1641 (2019).
- Jin, F. F. An equatorial ocean recharge paradigm for ENSO. Part I: Conceptual model. *J. Atmos. Sci.* **54**, 811–829 (1997).
- Fang, X. H. & Mu, M. A. A three-region conceptual model for central Pacific El Niño including zonal advective feedback. *J. Clim.* **31**, 4965–4979 (2018).
- Capotondi, A. ENSO diversity in the NCAR CCSM4. *J. Geophys. Res.* **118**, 4755–4770 (2013).
- Chen, N., Fang, X. & Yu, J. Y. A multiscale model for El Niño complexity. *npj Clim. Atmos. Sci.* **5**, 16 (2022).
- Jadhav, J., Panickal, S., Marathe, S. & Ashok, K. On the possible cause of distinct El Niño types in the recent decades. *Sci. Rep.* **5**, 17009 (2015).
- Izumo, T. et al. On the physical interpretation of the lead relation between Warm Water Volume and the El Niño Southern Oscillation. *Clim. Dyn.* **52**, 2923–2942 (2019).
- Hu, S., Fedorov, A. V., Lengaigne, M. & Guilyardi, E. The impact of westerly wind bursts on the diversity and predictability of El Niño events: an ocean energetics perspective. *Geophys. Res. Lett.* **41**, 4654–4663 (2014).



53. Fedorov, A. V., Hu, S., Lengaigne, M. & Guilyardi, E. The impact of westerly wind bursts and ocean initial state on the development, and diversity of El Niño events. *Clim. Dyn.* **44**, 1381–1401 (2015).
54. Chen, D. et al. Strong influence of westerly wind bursts on El Niño diversity. *Nat. Geosci.* **8**, 339–345 (2015).
55. Cane, M. A., Zebiak, S. E. & Dolan, S. C. Experimental forecasts of El Niño. *Nature* **321**, 827–832 (1986).
56. Penland, C. & Magorian, T. Prediction of Niño 3 sea surface temperatures using linear inverse modeling. *J. Clim.* **6**, 1067–1076 (1993).
57. Palmer, T. N. et al. Development of a European multimodel ensemble system for seasonal-to-interannual prediction (demeter). *Bull. Am. Meteorol. Soc.* **85**, 853–872 (2004).
58. Chekroun, M. D., Kondrashov, D. & Ghil, M. Predicting stochastic systems by noise sampling, and application to the El Niño–Southern Oscillation. *Proc. Natl. Acad. Sci. USA* **108**, 11766–11771 (2011).
59. Saha, S. et al. The NCEP climate forecast system version 2. *J. Clim.* **27**, 2185–2208 (2014).
60. Chapman, D., Cane, M. A., Henderson, N., Lee, D. E. & Chen, C. A. A vector autoregressive ENSO prediction model. *J. Clim.* **28**, 8511–8520 (2015).
61. Feng, Q. Y. et al. ClimateLearn : A machine-learning approach for climate prediction using network measures. Preprint at <https://gmd.copernicus.org/preprints/gmd-2015-273/> (2016).
62. Lu, Z., Yuan, N. & Fu, Z. Percolation phase transition of surface air temperature networks under attacks of El Niño/La Niña. *Sci. Rep.* **6**, 26779 (2016).
63. Rodríguez-Mendez, V., Eguiluz, V. M., Hernández-García, E. & Ramasco, J. J. Percolation-based precursors of transitions in extended systems. *Sci. Rep.* **6**, 29552 (2016).
64. Meng, J., Fan, J., Ashkenazy, Y., Bunde, A. & Havlin, S. Forecasting the magnitude and onset of El Niño based on climate network. *New. J. Phys.* **20**, 043036 (2018).
65. Noteboom, P. D., Feng, Q. Y., Lopez, C., Hernández-García, E. & Dijkstra, H. A. Using network theory and machine learning to predict El Niño. *Earth Syst. Dyn.* **9**, 969–983 (2018).
66. Ham, Y. G., Kim, J. H. & Luo, J. J. Deep learning for multi-year ENSO forecasts. *Nature* **573**, 568–572 (2019).
67. Meng, J. et al. Complexity based approach for El Niño magnitude forecasting before the spring predictability barrier. *Proc. Natl. Acad. Sci. USA* **117**, 177–183 (2019).
68. De Castro Santos, M. A., Vega-Oliveros, D. A., Zhao, L. & Berton, L. Classifying El Niño–Southern Oscillation combining network science and machine learning. *IEEE Access* **8**, 55711–55723 (2020).
69. Petersik, P. J. & Dijkstra, H. A. Probabilistic forecasting of El Niño using neural network models. *Geophys. Res. Lett.* **47**, e2019GL086423 (2020).
70. Hassanibesheli, F., Kurths, J. & Boers, N. Long-term ENSO prediction with echo-state networks. *Environ. Res.: Clim.* **1**, 011002 (2022).
71. Guilyardi, E. et al. A first look at ENSO in CMIP5. *CLIVAR Exch.* **17**, 29–32 (2012).
72. Guilyardi, E. et al. New strategies for evaluating ENSO processes in climate models. *Bull. Amer. Met. Soc.* **93**, 235–238 (2012).
73. Capotondi, A., Ham, Y. G., Wittenberg, A. T. & Kug, J. S. Climate model biases and El Niño Southern Oscillation (ENSO) simulation. *US CLIVAR Var.* **13**, 21–25 (2015).
74. Guilyardi, E. et al. Fourth CLIVAR workshop on the evaluation of ENSO processes in climate models: ENSO in a changing climate. *Bull. Am. Meteor. Soc.* **97**, 817–820 (2016).
75. Shin, N. Y. et al. More frequent central Pacific El Niño and stronger eastern Pacific El Niño in a warmer climate. *npj Clim. Atmos. Sci.* **5**, 101 (2022).
76. Gozolchiani, A., Havlin, S. & Yamasaki, K. Emergence of El Niño as an autonomous component in the climate network. *Phys. Rev. Lett.* **107**, 148501 (2011).
77. Huang, B. et al. Extended reconstructed sea surface temperature, version 5 (ERSSTv5): upgrades, validations, and intercomparisons. *J. Clim.* **30**, 8179–8205 (2017).
78. Kalnay, E. et al. The NCEP/NCAR 40-year reanalysis project. *Bull. Am. Meteorol. Soc.* **77**, 437–471 (1996).
79. Behringer, D. W., Ji, M. & Leetmaa, A. An improved coupled model for ENSO prediction and implications for ocean initialization. Part I: The ocean data assimilation system. *Mon. Weather Rev.* **126**, 1013–1021 (1998).
80. Kirtman, B. P. et al. The North American multimodel ensemble: phase-1 seasonal-to-interannual prediction; phase-2 toward developing intraseasonal prediction. *Bull. Am. Meteorol. Soc.* **95**, 585–601 (2014).

## ACKNOWLEDGEMENTS

J.L. thanks the “Brazil East Africa Peru India Climate Capacities (B-EPICC)” project, which is part of the International Climate Initiative (IKI) of the German Federal Ministry for Economic Affairs and Climate Action (BMWK) and implemented by the Federal Foreign Office (AA).

## AUTHOR CONTRIBUTIONS

J.L., A.B., and H.J.S. designed research; J.L. performed research; J.L. and A.B. analyzed data; J.L., A.B., and H.J.S. wrote the paper.

## FUNDING

Open Access funding enabled and organized by Projekt DEAL.

## COMPETING INTERESTS

The authors declare no competing interests.

## ADDITIONAL INFORMATION

**Supplementary information** The online version contains supplementary material available at <https://doi.org/10.1038/s41612-023-00519-8>.

**Correspondence** and requests for materials should be addressed to Josef Ludescher.

**Reprints and permission information** is available at <http://www.nature.com/reprints>

**Publisher's note** Springer Nature remains neutral with regard to jurisdictional claims in published maps and institutional affiliations.



**Open Access** This article is licensed under a Creative Commons Attribution 4.0 International License, which permits use, sharing, adaptation, distribution and reproduction in any medium or format, as long as you give appropriate credit to the original author(s) and the source, provide a link to the Creative Commons license, and indicate if changes were made. The images or other third party material in this article are included in the article's Creative Commons license, unless indicated otherwise in a credit line to the material. If material is not included in the article's Creative Commons license and your intended use is not permitted by statutory regulation or exceeds the permitted use, you will need to obtain permission directly from the copyright holder. To view a copy of this license, visit <http://creativecommons.org/licenses/by/4.0/>.

© The Author(s) 2023